A presumed pdf model for droplet evaporation/condensation in complex flows

By S. Apte AND S. Ghosal†

1. Motivation and objectives

In many multiphase flow problems, the condensed phase (liquid or solid) exists in the form of a cloud of droplets of heterogeneous size in an ambient gas undergoing time dependent (often turbulent) motion. One example is the problem of the formation and growth of ice crystals in the "contrails" of aircraft [Paoli *et al.* 2002 - henceforth cited as CTR-SP0]. Other examples include, atmospheric aerosols (Binkowski & Shankar, 1995), rain drops in clouds (Shaw 2003), and, the fuel vapor from evaporating drops of hydrocarbon fuel in spray combustion engines (Moin & Apte 2005). In order to be specific, we shall assume here that the condensed phase is a liquid that undergoes evaporation.

The need for modeling the spray arises in both LES and DNS. In DNS, the size of a computational grid is typically within an order of magnitude of the Kolmogorov scale. However, if particle sizes and the average distance between particles is much smaller than this, then clearly some kind of a statistical description of the particles need to be adopted so as not to increase the computational effort by many orders of magnitude. In LES the size of the computational grid is somewhere intermediate between the integral scale and the Kolmogorov scale. Here once again some statistical modeling is needed if particle sizes and the distance between them are much smaller than the LES grid.

In this report the statistical description based on a 'presumed pdf' (henceforth PPDF) outlined in CTR-SP02 is worked out in detail for a specific evaporation model and for a lognormal form of the presumed pdf. The predictions are checked against a full numerical simulation that does not involve any statistical modeling. The general formalism had been presented in Sec 4.1 of CTR-SP02 and need not be reported here. We will assume the results presented in that earlier report and also adopt the notation used there.

2. The Model

The simplest nontrivial model follows from assuming that the "presumed pdf" is a two parameter distribution depending on the first two moments m_1 and m_2 in addition to the droplet density $N_p = m_0$. Then the time evolution of N_p, m_1 and m_2 are described by equations (4.2) and (4.3) of CTR-SP02‡ with the series of moment equations truncated at $k = 2$. In order to obtain explicitly the source terms we need to specify (a) the analytical form of the presumed pdf and (b) the evaporation/condensation model.

2.1. *Evaporation Law*

We will assume that the fluid droplets are spherical and at a fixed temperature T_0. Further, the local thermal field around a droplet is described by spherically symmetric

† Northwestern University

‡ please note that (4.3) in CTR-SP02 has a typographic error, it should read $\frac{\partial m_k}{\partial t} + \nabla \cdot (m_k \mathbf{u}) = k \int_0^\infty r^{k-1} n_p \dot{r}\, dr$

solutions of $\nabla^2 T = 0$ with the far field temperature matched to $T(\mathbf{x}, t)$, the temperature at the location of the particle in the absence of the drop. Any cooling effect on the gas due to particle evaporation is neglected. The rate of inflow of heat to the droplet can then be easily calculated. If one assumes that this energy is expended in raising the temperature of the liquid to its boiling point and evaporating some of the liquid, then, the change of droplet radius is given by

$$\frac{dr}{dt} = -\frac{\Lambda(T - T_0)}{r} \tag{2.1}$$

where Λ is a constant determined by properties of the gas and the liquid:

$$\Lambda = \frac{k_g/\rho_\ell}{L + C_\ell(T_* - T_0)} \tag{2.2}$$

where k_g is the thermal diffusivity of the gas, L is the latent heat of vaporization, ρ_ℓ is the liquid density, C_ℓ is the liquid specific heat and T_* is the temperature at the boiling point.

2.2. *The Presumed PDF*

The form of the presumed pdf ϕ for the distribution of particle sizes will be assumed lognormal;

$$n_p = \phi(r; m_0, m_1, m_2) = \frac{N_p}{\sigma r\sqrt{2\pi}} \exp\left[-\frac{1}{2\sigma^2}\left(\ln(r/r_p)\right)^2\right] \tag{2.3}$$

where the parameters N_p, r_p and σ^2 are easily seen to be related to m_0, m_1 and m_2 through the relations

$$m_0 = N_p; \qquad m_1 = N_p r_p \exp(\sigma^2/2); \qquad m_2 = N_p r_p^2 \exp(2\sigma^2). \tag{2.4}$$

The mean particle radius $\langle r\rangle$ and the variance of the particle radius $\langle \Delta r^2\rangle$ may be easily shown to be related to r_p and σ by the relations

$$\sigma^2 = \ln\left[1 + \frac{\langle \Delta r^2\rangle}{\langle r\rangle^2}\right]; \qquad r_p^2 = \frac{\langle r\rangle^4}{\langle r\rangle^2 + \langle \Delta r^2\rangle}. \tag{2.5}$$

If $\langle \Delta r^2\rangle \ll \langle r\rangle^2$ we get $r_p \approx \langle r\rangle$ and $\sigma^2 \approx \langle \Delta r^2\rangle / r_p^2 = \langle \Delta r^2\rangle / \langle r\rangle^2$; the variance normalized by the square of the mean.

2.3. *Time Evolution of Distribution Parameters*

The right hand sides of equations (4.3) in CTR-SP02 may be explicitly evaluated using the presumed pdf (2.3) and the evaporation law (2.1). Further, using (2.4) the equations can be transformed into a form that uses N_p, r_p and σ^2 in place of m_0, m_1 and m_2 as dependent variables:

$$\frac{D}{Dt}\left(\frac{N_p}{\rho}\right) = 0, \qquad \frac{Dr_p}{Dt} = \mathcal{S}_r, \qquad \frac{D\sigma^2}{Dt} = \mathcal{S}_\sigma, \tag{2.6}$$

where the source terms $\mathcal{S}_r$ and $\mathcal{S}_\sigma$ are given by

$$\mathcal{S}_r = -\frac{\Lambda(T - T_0)}{r_p}\left\{2 - \exp(-2\sigma^2)\right\}, \qquad \mathcal{S}_\sigma = \frac{2\Lambda(T - T_0)}{r_p^2}\left\{1 - \exp(-2\sigma^2)\right\}. \tag{2.7}$$

Using the continuity equation, the equations (2.6) can also be expressed in conservative form, which may be more suited for numerical methods such as finite volume approaches. Equations (2.6) determine the value of the parameters N_p, r_p and σ^2 at any time.

Knowing these three parameters at any given point in space, "P", the PDF of drop sizes in the neighborhood of "P" is determined by (2.3). Thus, any desired quantity related to the interaction between the gas phase variables (resolved) and condensed phase (unresolved) may be calculated. For example, if droplet evaporation is a source of combustible vapors, then we may write

$$\rho \frac{DY_F}{Dt} = -\omega + \nabla \cdot (k_F \nabla Y_F) + S \tag{2.8}$$

where Y_F is the vapor mass fraction, ω is the rate of removal of vapor mass due to chemical reaction, k_F is a diffusion coefficient and the source term due to liquid evaporation from the droplets is

$$S = -\int_0^\infty n_p \dot{r}(4\pi r^2)\rho_\ell \, dr = 4\pi\Lambda\rho_\ell(T - T_0)N_p r_p \exp(\sigma^2/2). \tag{2.9}$$

To obtain the expression on the right hand side, $\dot{r}$ and n_p was substituted from (2.1) and (2.3) the integral was evaluated in order to sum the contributions from all droplet sizes. Equations (2.6) and (2.8) may be solved together to account for the gas as well as the condensed phase without the need for following the motion of each particle in the condensed phase.

2.4. *Physical Interpretation*

The first of equations (2.6) simply means that the total number of droplets in a material volume of fluid does not change. The density in the denominator takes account of the fact that the volume of the material element could vary if the flow is compressible. At first sight this conclusion may seem to be in conflict with the fact that droplets may evaporate completely! However, this paradox is only superficial since in the language of PDFs droplets never evaporate "completely", rather, the distribution function n_p shifts continuously towards smaller and smaller particle sizes ($r_p \to 0$) so that the total mass in the condensed phase goes arbitrarily close to zero. Thus, the right hand side of (2.9) would be "machine zero" after sufficient time has evolved; whether one describes this situation by saying "all droplets have evaporated" or the "distribution function has become extremely localized around $r = 0$" is of course just a matter of linguistics.

The interpretation of the second of equations (2.6) is clearest if one considers the initial PDF of drop sizes to be narrowly peaked around the mean size: $\langle \Delta r^2 \rangle \ll \langle r \rangle^2$. In this case, as pointed out before, $r_p \approx \langle r \rangle$ and $\sigma^2 \approx \langle \Delta r^2 \rangle / r_p^2 = \langle \Delta r^2 \rangle / \langle r \rangle^2 \ll 1$. Therefore, the source terms of the equations for r_p and σ^2 in (2.6) may be simplified:

$$\frac{Dr_p}{Dt} = \mathcal{S}_r \approx -\frac{\Lambda(T - T_0)}{r_p}(1 + 2\sigma^2), \qquad \frac{D\sigma^2}{Dt} = \mathcal{S}_\sigma \approx \frac{4\Lambda(T - T_0)}{r_p^2}\sigma^2. \tag{2.10}$$

Thus, if $\sigma = 0$ initially, it remains zero and the mean droplet size remains exactly equal to the size of any droplet in the monodisperse cluster since the evolution equation for r_p is the same as (2.1) for an individual drop. However, if σ^2 is small but nonzero, these equations predict (a) the mean of the distribution shifts to the left *faster* than the radius of an individual droplet of radius r_p (b) the variance of the distribution increases rapidly. The physical reason behind these predictions may be found in the evaporation law (2.1) according to which small droplets get smaller *faster* than large ones. Indeed, if one considers three droplets of radii $r_1 < r_2 < r_3$ then since r_1 decreases faster than r_3, $r_1 - r_3$ would get larger with time, that is the spread of the distribution increases. Also, if initially r_2 was the mean of r_1 and r_3, at later times the mean would be less than r_2,

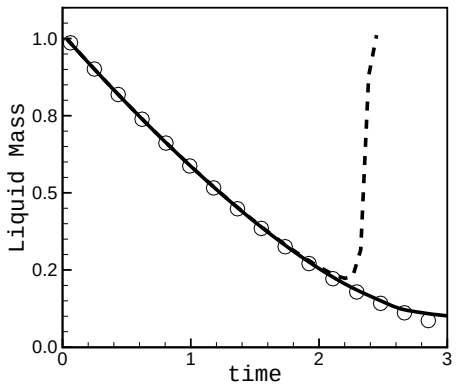

FIGURE 1. Temporal evolution of total mass of droplets in a Taylor-vortex flow for $\sigma = 0.1$: $\circ$ DNS, – – – model with $\mathcal{S}_\sigma$ given by equation (2.6), ——— model with $\mathcal{S}_\sigma$ given by equation (3.5).

that is the average of the distribution decreases faster than an average sized drop. This is indeed what equations (2.10) predicts.

3. A Problem with the model and its resolution

Figure 1 shows the change of total mass in the liquid phase as predicted by equations (2.6) in a swirling 'Taylor-vortex' flow with an inhomogeneous initial temperature distribution. The details of the simulation are discussed in the following section. Here it suffices to point out that the predicted liquid mass is in close agreement with the full DNS of the system until very late times when apparently some kind of instability develops causing the liquid mass to *increase* rapidly - a completely unphysical prediction - since each individual droplet is evaporating!

3.1. *Physical mechanism for anomalous growth*

The instability is not a numerical one but its source is in the equations (2.6) themselves. To see this, first note that the total volume of liquid in the condensed phase in the entire domain (Ω) at a given instant may be expressed as

$$V(t) = \int_\Omega dV \int_0^\infty n_p \frac{4}{3}\pi r^3 \, dr = \frac{4}{3}\pi \int_\Omega dV \; N_p r_p^3 \exp\left(\frac{9}{2}\sigma^2\right) \tag{3.1}$$

where the second equality follows on substituting the expression (2.3) for n_p and performing the radial integration. As a particular case, suppose that system is homogeneous (N_p, r_p, σ are position independent). Further suppose there is no flow so that $D/Dt = \partial/\partial t$ in (2.6). In this case it is easy to show that

$$\frac{1}{V}\frac{dV}{dt} = \frac{3\Lambda(T - T_0)}{r_p^2}[1 - 2\exp(-2\sigma^2)]. \tag{3.2}$$

When $\sigma \ll 1$ the right hand side is negative (assuming $T > T_0$ everywhere) but as σ becomes large the sign of the term in [ ] changes and the volume of the condensed phase

starts to increase! This is the source of the observed late time instability apparent in figure 1.

3.2. *Resolution of the difficulty*

First note that $V(t)$ is related to the third moment $m_3(\mathbf{x},t)$ of the distribution:

$$V(t) = \frac{4}{3}\pi \int_\Omega dV\ m_3(\mathbf{x},t). \tag{3.3}$$

Now according to equation (4.3) of CTR-SP02 m_3 actually has an evolution equation:

$$\frac{\partial m_3}{\partial t} + \nabla\cdot(m_3\mathbf{u}) = 3\int_0^\infty r^2 n_p \dot{r}\ dr \tag{3.4}$$

with a source term that is always negative as long as $\dot{r} < 0$. The problem with our model is that we *discarded* this moment equation (together with all higher moments) in order to achieve a "closure". Thus, in the current model, the behavior of "m_3" is a derived quantity determined by the dynamics of m_0, m_1, m_2 and the presumed PDF, and there is nothing in those lower order equations to ensure that V would decrease for evaporating droplets.

The nature of the difficulty also suggests a resolution. If one were to adopt a moment closure at the level of m_3 and assume that the presumed PDF $\phi = \phi(m_0, m_1, m_2, m_3)$, then the equation for m_3 would ensure that V does not increase. Actually we can achieve the same result within the lognormal formalism itself, if we notice that the lognormal form of the presumed PDF with three independent parameters requires that we retain *any three* of the equations of the moment hierarchy, *not necessarily the first three*! We will therefore modify our closure assumption by enforcing the moment equations for m_0, m_1 and m_3 and dropping all the rest. This is no more or no less justified than our original closure but it does have the advantage that the physically important moment m_3 is calculated directly from its evolution equation.

With this modification, the form of our basic model (2.6) remains unaltered, except for the formula for the source term which now becomes:

$$\mathcal{S}_\sigma = \frac{2}{3}\frac{\Lambda(T-T_0)}{r_p^2}\left\{2 - \exp(-2\sigma^2) - \exp(-4\sigma^2)\right\}. \tag{3.5}$$

If the calculation leading up to (3.2) is repeated with the modified source term, it is readily verified that this time $\dot{V} < 0$. In fact one need not assume statistical homogeneity or that $\mathbf{u} = 0$, in general,

$$\frac{dV}{dt} = -4\pi \int_\Omega r_p N_p \Lambda(T-T_0)\exp(\sigma^2/2)\ d\mathbf{x} \tag{3.6}$$

which implies that $\dot{V} < 0$ as long as $T > T_0$ everywhere. Thus, stability is assured and indeed when the simulation is repeated with the new source term (3.5), the liquid mass decreases monotonically and in good agreement with experimental data as shown in figure 1.

Another interesting property of equation (3.5) is that when $\sigma^2 \ll 1$, both the right hand side of (3.5) and the second of equations (2.10) evaluate to

$$\mathcal{S}_\sigma \approx \frac{4\Lambda(T-T_0)}{r_p^2}\sigma^2. \tag{3.7}$$

Thus, at low dispersions, enforcing the equation for m_3 automatically enforces the equation for m_2, until the dispersion gets very large.

4. Numerical Experiments

The PPDF model (2.6) with the modified source term (3.5) is used to simulate a cloud of evaporating droplets in the presence of a temperature gradient in a two-dimensional decaying Taylor vortex flow. Preliminary results are also presented for the case of forced isotropic turbulence in a box. The flows considered here are periodic and solved in a periodic box of dimensionless length 2π. The reference length and velocity scales used in the computation are 1 m and 1 m/s, respectively, giving a reference time-scale of 1 s. Results are compared with direct numerical simulations using Lagrangain tracking of all droplets.

4.1. *Decaying Taylor Vortex*

The initial conditions for the velocity components are:

$$u(x, y, 0) = -\pi \cos x \sin y \tag{4.1}$$

$$v(x, y, 0) = \pi \sin x \cos y \tag{4.2}$$

and initial temperature distribution is

$$T = T_{min} + \Delta T \, |1 - x/\pi| \tag{4.3}$$

$$\Delta T = T_{max} - T_{min} \tag{4.4}$$

We use isopropyl alcohol as the liquid phase, and we take $T_{min} = 355\ K$ (the boiling point of isopropyl alcohol) and $\Delta T = 2250\ K$, representative of the typical temperatures achieved in turbulent combustion. Figure 2 shows the initial streamlines and the temperature field. The Reynolds number is $Re = 50,000$ and we use 32×32 grid points for this two-dimensional calculation. To test the model's predictions we performed a DNS by tracking 122880 droplets which were initially randomly distributed over the computational domain. Approximately 120 droplets were obtained per control volume providing statistically meaningful results. For DNS, the initial droplet sizes in each control volume were sampled from the lognormal distribution (2.3) with a mean droplet radius of 250 microns. Two cases with different variances ($\sigma = 0$ and 0.1) were investigated. Using the properties of isopropyl alcohol (Reid *et al.* 1987) the droplet life-time of a $r_0 = 250$ micron size drop can be estimated as,

$$t_e = \frac{r_0^2}{2\Lambda \, (T_{max} - T_0)} \approx 0.23\, s \tag{4.5}$$

This is shorter than an eddy turn over time ($\sim$ 1 s) and much shorter than the viscous decay time of the eddies ($\sim 157,000$ sec), so that for the duration of the computation, the vortices are essentially stationary in time.

4.1.1. *Case 1:* $\sigma = 0$

For this case, at the initial time, the computational domain was seeded with droplets of a uniform size (250 μm). Figure 3 shows the time evolution of the droplet radius averaged over the entire domain, the total liquid mass in the droplets, and the fuel vapor mass fraction obtained from DNS and the model. All of these global averages are seen to be predicted very accurately by the model.

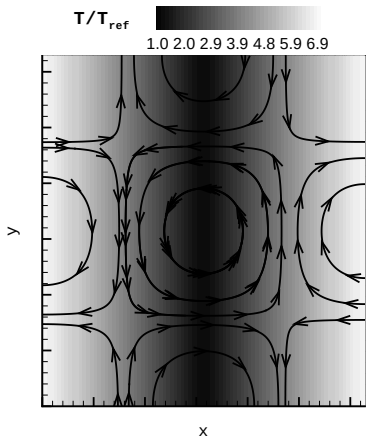

FIGURE 2. Initial streamlines and temperature distribution in a 2D Taylor-vortex flow: $T_{ref} = T_{min}$.

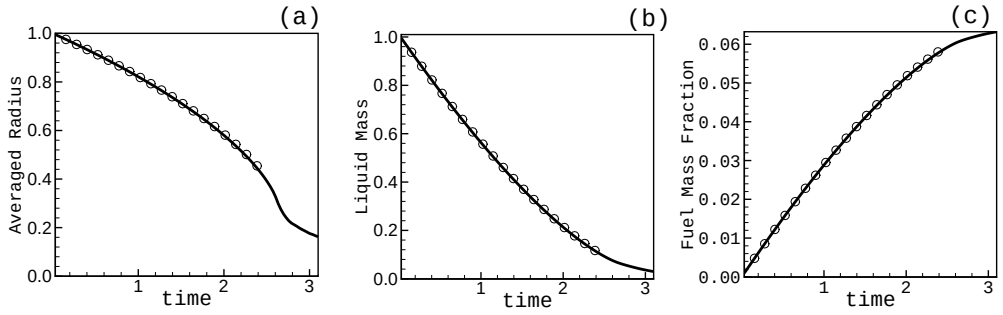

FIGURE 3. Temporal evolution of global quantities for $\sigma = 0$: ∘ DNS, ——— PPDF, (a) Volume average of mean droplet radius (b) total liquid mass (both normalized by respective initial values) and (c) fuel mass fraction, Y_F.

4.1.2. *Case 2:* $\sigma = 0.1$

Keeping the flow conditions the same as in case 1, we introduce a small variance ($\sigma = 0.1$) in the initial droplet size distribution. For DNS, droplets in each control volume were sampled from a lognormal distribution giving a scatter of ± 50 μm around the mean droplet radius of 250 μm. Figure 4 shows the instantaneous distribution of fuel mass fraction obtained from DNS and the model at a later time. The time-evolution of the total liquid mass and fuel mass fraction in the computational domain (figure 5) also show good agreement with the DNS. However, at large times, the mean droplet radius obtained using PPDF is lower than that of DNS (figure 5). This could be an artifact of our sampling procedure, since in DNS particles that have become too small are discarded so they are no longer counted in the calculation of the mean. The loss of these small values could upwardly bias the mean.

Next we calculate the average droplet radius within each control volume. Figure 6 shows the scatter plot of the mean droplet radius at each control volume obtained from the DNS and the model. At $t = 0$, the mean droplet radii in all control volumes obtained

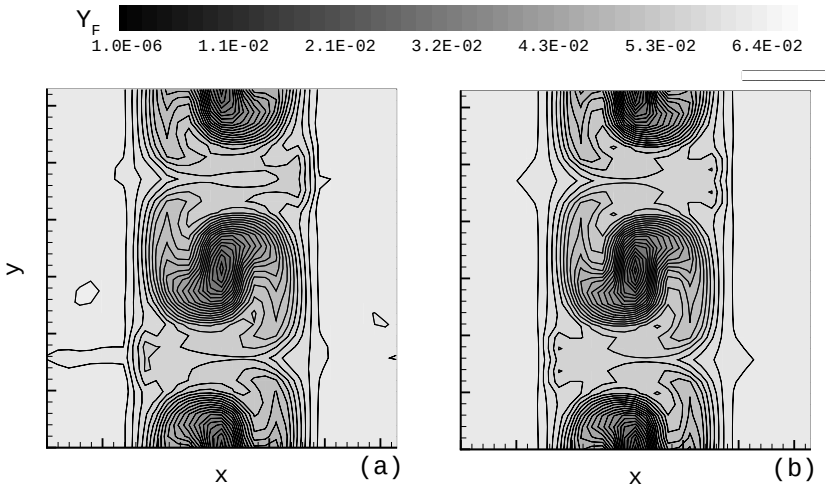

FIGURE 4. Contour plot of fuel mass fraction Y_F at $t = 2.5$ for $\sigma = 0.1$: (a) DNS, (b) PPDF

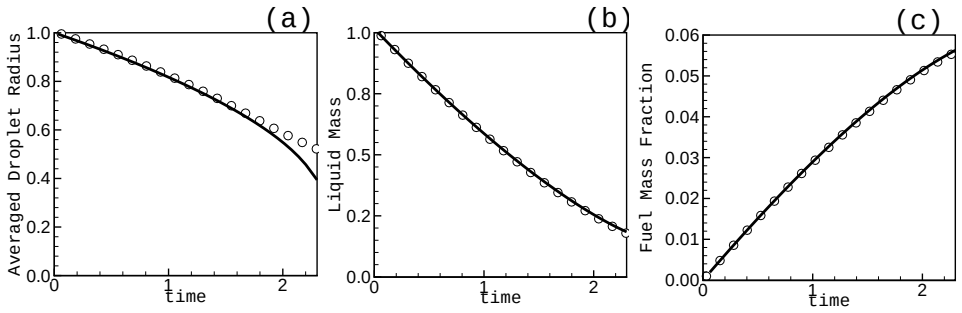

FIGURE 5. Temporal evolution of global quantities for $\sigma = 0.1$: ∘ DNS, —— PPDF, (a) Volume average of droplet radius, (b) total liquid mass (both normalized by respective initial values) and (c) mean fuel mass fraction in volume, $\langle Y_F \rangle$.

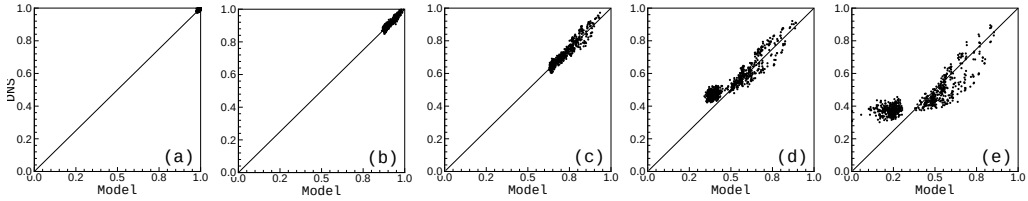

FIGURE 6. Correlation analysis between the DNS and PPDF for droplet radius averaged over a control volume. Scatter plot shows mean radius at each grid cell: a) $t = 0$, b) $t = 0.75$, c) $t = 1.5$, d) $t = 2$, e) $t = 2.5$

from both DNS and model are the same. The small scatter is due to discrete sampling of droplet sizes in DNS. With time, the mean droplet size in certain control volumes decreases more rapidly due to evaporation and the scatter plot shifts to the left towards zero radius, but the predictions from the two simulations are closely correlated. At large

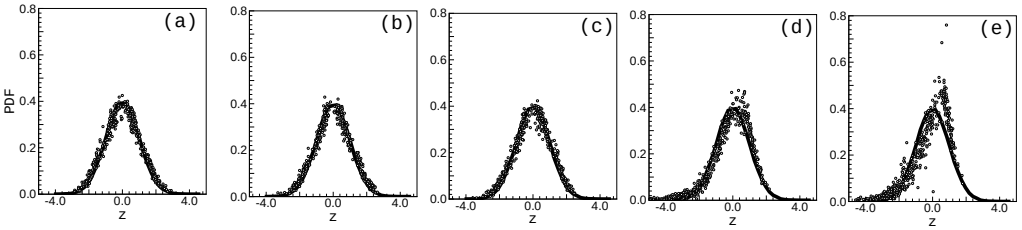

FIGURE 7. Test of the validity of the lognormal distribution of droplet radius; plot of $z = (\ln r - \ln r_p)/\sigma$ (x-axis) against PDF (y-axis), ∘ PPDF: at (a) $t = 0$ (b) $t = 0.75$ (c) $t = 1.5$ (d) $t = 2$ (e) $t = 2.5$, ——— Standard normal distribution (zero mean & unit variance).

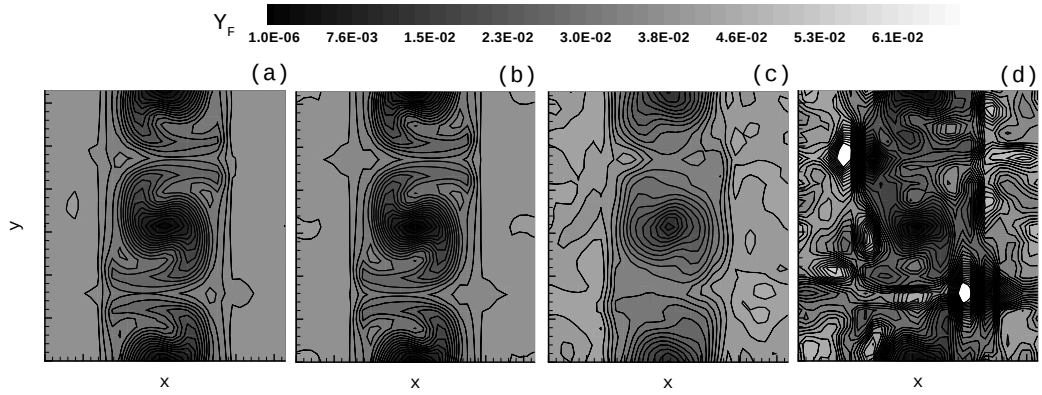

FIGURE 8. Instantaneous profiles of fuel mass fraction. Comparison of PPDF predictions with standard Lagrangian Parcel Tracking (LPT) at $t = 2.4$: a) DNS, b) PPDF, c) LPT1; 6144 parcels, d) LPT2; 256 parcels.

times, the mean droplet radius from DNS is generally higher than that obtained from the model. This is partly because of the fact that droplets smaller than a threshold were removed in the DNS resulting in higher mean of the droplet radius. Local liquid mass, on the other hand, shows good correlation between the model and the DNS mainly because droplets of size less than the threshold contribute little to the mass in a control volume.

Figure 7 shows the pdf of the variable $z = (\ln r - \ln r_p)/\sigma$ which should follow the unit normal distribution if r is distributed lognormally. The data was obtained from the DNS at times corresponding to those in figure 6. From the DNS, we collect all droplets in a control volume, and use the data to determine r_p and σ for that control volume. Then the variable z is calculated for each particle, the results binned and plotted. The same procedure is repeated for each control volume. As shown in figure 7, initially the pdf collapses on top of the standard normal distribution. With time, there are some small deviations but the distribution does remain close to lognormal until most of the liquid has evaporated.

4.1.3. *PPDF or Lagrangian Parcels Tracking (LPT)?*

In simulations of practical gas-turbine combustor, the spray is represented by computational particles or 'parcels' each representing a fixed number of droplets. Each parcel carries with it properties: velocity, mass, radius, temperature etc. equal to that of some

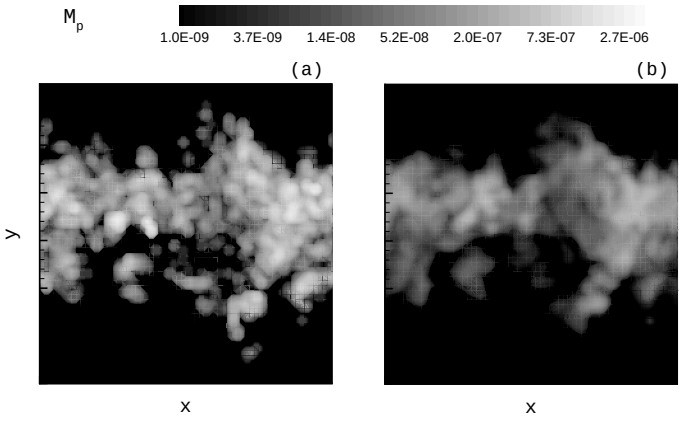

FIGURE 9. Instantaneous profiles of liquid mass dispersed in isotropic turbulence: a) DNS, b) PPDF

'average' particle in the cloud that it represents (Apte *et al.* 2003a, Apte *et al.* 2003b). Replacing a large clump of particles by a single 'proxy' in this way reduces the computational cost to manageable levels. The accuracy of the algorithm as well as its computational cost is inversely correlated to the number of particles that a parcel represents. In order to compare the PPDF model with the LPT approach in regards to accuracy as well as computational cost, two separate simulations were run with the LPT method using the conditions corresponding to case 2 of the Taylor-vortex flow. We will call these cases (a) LPT1: 3072 parcels each representing 40 droplets and (b) LPT2: 128 parcels each representing 960 droplets. They both correspond to the same number (122, 880) of droplets present in the DNS. These numbers are typical of a realistic spray simulation in complex combustors (Moin & Apte 2005). Figure 8 shows the instantaneous distributions of fuel vapor mass fraction obtained from DNS, PPDF, LPT1, and LPT2. It is seen that the accuracy in predicting the evolution of fuel mass fraction degrades considerably as one goes from 40 to 960 drops per parcel. Table 4.1.3 shows the comparison of CPU time per 100 iterations on a single processor of Origin2000 for the four different approaches. It should be noted that the PPDF and LPT1 have comparable computational cost, with the PPDF approach actually producing somewhat better agreement with DNS at a cost that is slightly lower than the LPT1 simulation.

Method	DNS	PPDF	LPT1	LPT2
CPUs in second per 100 iterations	1200	75	85	50

4.2. *Forced Isotropic Turbulence*

The PPDF model was used to simulate forced isotropic turbulence with temperature gradients at $Re_\lambda = 40$ on a 64^3 grid. The initial temperature profile was chosen as

$$T = T_{min} + \Delta T\,|1 - y/\pi| \tag{4.6}$$

where $\Delta T = T_{max} - T_{min} = 2000\ K$ and $T_{min} = 700\ K$. The configuration is representative of the interaction between a turbulent flame and a sprinkler system. The droplets that are introduced in a narrow band of thickness $\Delta y = 0.03 \times (2\pi)$ around $y = 0$. They may be thought of as originating from a sprinkler at $y = 0$ and being subsequently

convected by the turbulent flow as they evaporate and cool the system. Figure 9 shows an instantaneous map of the liquid mass in droplets obtained from the DNS and the model. Preliminary results show good agreement with the DNS data. A more systematic analysis for this turbulent flow case is in progress.

5. Discussion

The model developed here is based on certain assumptions which are valid to a greater or lesser approximation depending on the physical system being described. Let us bring together here these various assumptions, discuss under what conditions they are valid and how the current theory may be expanded (if possible) when the assumptions fail to be valid.

First, we wrote down a continuity equation in phase space for the PDF $n_p(\mathbf{x}, r, t)$: (4.3) of CTR-SP02. This equation is valid provided that

(a) the external field $\mathbf{u}$ varies on a length scale that is very much larger than Δ, the scale on which n_p itself varies.

(b) there exists no processes that would result in abrupt changes in particle radii (i.e. collisions, coalesence and break up of droplets).

(c) the particles move with the local flow velocity.

Both (a) and (b) are reasonable if $a \ll d \ll \eta$ where a is a characteristic particle radius, d is a typical separation and η is the Kolmogorov scale. If $d \sim \eta$ and one is solving a DNS then the PDF approach is of course superfluous since one has only a few particles per grid and one might as well track them individually and not rely on any modeling. If on the other hand one is describing the system at a courser level, such as an LES then $\Delta \gg d$ and $d \sim \eta$ or $d \gg \eta$. In this case the velocity in (4.3) of CTR-SP02 need to be decomposed into a slowly varying part and a second rapidly varying term. If one assumes that the latter (the rapidly varying part) has a net diffusive effect (the "Fokker-Planck Approximation") then the moment equations get modified through the appearance of a term $\alpha \nabla^2 m_k$ (where $\alpha > 0$) on the right hand side and $\mathbf{u}$ is identified as the smooth part of the velocity field. Thus, such a modification of the theory would extend it to situations such as LES where $\mathbf{u}$ has a smooth and a fluctuating component. If $a \sim d$ then assumption (b) is no longer valid because of collisions between particles. Unlike the case of collisions between rigid spheres, there exists no simple "collision operator" for the coalescence and break up of fluid drops. In a turbulent fluid statistical break up models such as those due to Kolmogorov predict an equilibrium distribution n_p^{eq} that is lognormal (Kolmogorov 1941, Gorokhovski 2001). If the system is not very far from equilibrium a linearized collision operator $(n_p - n_p^{eq})/\tau$ (where τ is a timescale parameter) may be used and the moment equations should be modified to account for such a term. The approximation is not likely to be valid far from equilibrium. Fortunately in many combustor systems there are separate zones characterizing droplet break up and evaporation and the current model might be useful in the latter zone while the break up region is handled by a different approach. The third assumption is the assumption of zero particle inertia. Its accuracy depends on the Reynolds number based on particle radius being small. The violation of this assumption leads to important phenomena that are well known (Reade & Collins 2000).

Secondly we assumed that the system has a "universal behavior" in the sense that the PDF has a certain prescribed form (such as lognormal) the only thing that varies with position and time are the finite set of moments $m_0, \ldots, m_n$ that specify the distribution.

Such 'self-similarity' is well known in systems with many degrees of freedom, the case of an ideal gas being a familiar example. In that case, the velocity distribution is "locally Maxwellian" everywhere, the parameters of the Maxellian obey certain moment equations which are the familiar Navier-Stokes-Fourier equations of classical gas dynamics. The self-similarity in the gas dynamic example follows from the smallness of the duration of collisions compared to the time between collisions. The smallness of the ratio of these two time-scales imply a collapse to a center manifold the evolution on which is described by the Navier-Stokes-Fourier equations. In our case, we do not have an asymptotic formalism such as the Chapman-Enskog development to systematically prove such a self-similar behavior but rather such behavior is assumed apriori, an assumption that is open to critique and subject to experimental test.

Thirdly we assumed lognormality and the evaporation law (2.1). These assumptions are the least fundamental and are only incidental to the particular test cases we chose to run. Both statistical arguments as well as experimental data exists to support the hypothesis that in dense two phase turbulent flows, the distribution of droplet sizes is well approximated by the lognormal distribution. Therefore, if we wish to model the zone beyond the break up zone where droplet evaporation dominates droplet break up, the lognormal assumption is a reasonable one at least for the particles entering our computational zone. Subsequently, evaporation could change the shape of the distribution, and the accuracy of the model would depend on whether or not droplet evaporation is essentially complete before substantial departure from lognormality becomes an issue. If it does become an issue, then one will need to replace ϕ by a more detailed model. Finally, equation (2.1) was chosen for illustrative purposes only. Models that capture much finer details of the particle evaporation or condensation process are well known in atmospheric physics. A modified evaporation law may also be desirable for a technical reason: equation (2.1) has the feature, that the radius of a droplet goes to zero in finite time $t = t_e$ which leads to a small denominator problem in equations (2.6) unless the droplet radius is artificially prevented from going to zero. However, a better way of avoiding the singularity is to modify the evaporation law (2.6), for example:

$$\frac{dr}{dt} = -\frac{\Lambda(T - T_0)}{r}\{1 - \exp(-r/b)\} \tag{5.1}$$

eliminates the finite time singularity. Here b is to be chosen as a length so small that the mass of liquid droplets of radius less than b is essentially zero for all physical purposes. The incorporation of these more complicated evaporation models involves only the practical difficulty of evaluating more complicated integrals for the source terms.

6. Acknowledgement

The work reported here was performed in the summer of 2004 during which time one of us (S.G.) was supported as a visitor at the Center for Turbulence Research.

REFERENCES

Apte, S. V., Gorokhovski, M. & Moin, P. 2003a LES of atomizing spray with stochastic modeling of secondary breakup *Int. J. Mult. Flow* **29**, 1503–1522.

Apte, S. V., Mahesh, K., Moin, P., & Oefelein, J.C. 2003b Large-eddy simulation of swirling particle-laden flows in a coaxial-jet combustor. *Int. J. Mult. Flow* **29**, 1311–1331.

BINKOWSKI, F.S., & SHANKAR, U. 1995 The regional particulate matter model 1. Model description and preliminary results, *J. Geo. Res.*, **100**: D12, 26191–26209.

GOROKHOVSKI M.A. 2001. The stochastic lagrangian model of drops breakup in the computation of liquid sprays, Atom. & Sprays, **11** (5): 505–520.

KOLMOGOROV A.N. 1941 On the log-normal distribution of particles sizes during breakup process, *Dokl. Akad. Nauk. SSSR, XXXI*, **2**: 99–101.

MOIN, P, & APTE, S.V. 2005 LES of multiphase reacting flows in complex combustors. *to appear in AIAA J.*

PAOLI, R., HÉLIE, J., POINSOT, T.J., & GHOSAL, S. 2002 Contrail formation in aircraft wakes using large-eddy simulations. *Proceedings of the CTR Summer Program*, Stanford University, Stanford.

READE, W. C. & COLLINS, L. R. 2000 Effect of preferential concentration on turbulent collision rates. *Phys. Fluids* **12**, 2530–2540.

REID, R.C., PRAUSNITZ, J.M., AND POLING, B.E., 1987 The Properties of Gases and Liquids. McGraw Hill, Boston.

SHAW, R. 2003 Particle-turbulence interactions in atmospheric clouds. *Ann. Rev. Fluid Mech.*, **35**, 183–227.